



Mao, K., Yang, Z., Li, J., Zhou, X., Li, X. and Hu, J. (2017) A novel colorimetric biosensor based on non-aggregated Au@Ag core-shell nanoparticles for methamphetamine and cocaine detection. *Talanta*, 175, pp. 338-346. (doi:[10.1016/j.talanta.2017.07.011](https://doi.org/10.1016/j.talanta.2017.07.011))

This is the author's final accepted version.

There may be differences between this version and the published version. You are advised to consult the publisher's version if you wish to cite from it.

<http://eprints.gla.ac.uk/146365/>

Deposited on: 22 August 2017

Enlighten – Research publications by members of the University of Glasgow  
<http://eprints.gla.ac.uk33640>

1                    **A Novel Colorimetric Biosensor Based on non-Aggregated**  
2                    **Au@Ag Core–Shell Nanoparticles for Methamphetamine and**  
3                    **Cocaine Detection**

4                    ***Kang Mao<sup>a</sup>, Zhugen Yang<sup>b</sup>, Junrong Li<sup>c</sup>, Xiaodong Zhou<sup>c</sup> Xiqing Li<sup>a,\*</sup> and Jiming***  
5                    ***Hu<sup>c</sup>***

6                    *<sup>a</sup> Laboratory for Earth Surface Processes, College of Urban and Environmental*  
7                    *Sciences, Peking University, Beijing 100871, China*

8                    *<sup>b</sup> Division of Biomedical Engineering, School of Engineering, University of Glasgow,*  
9                    *Oakfield Road, Glasgow G12 8LT, United Kingdom*

10                    *<sup>c</sup> Key Laboratory of Analytical Chemistry for Biology and Medicine (Ministry of*  
11                    *Education), College of Chemistry and Molecular Sciences, Wuhan University, Wuhan*  
12                    *430072, China*

13  
14  
15                    **Abstract**

16                    We report a novel colorimetric biosensor based on non-aggregation Au@Ag  
17                    core-shell nanoparticles to detect methamphetamine and cocaine. The biosensor  
18                    consisted of a reporter probe (RP) that is a specific single-stranded DNA (ssDNA)  
19                    sequence coated on Au@Ag nanoparticles, a capture probe (CP) conjugated with  
20                    magnetic beads, and an illicit drug-binding DNA aptamer (Apt). Au@Ag  
21                    nanoparticles were synthesized by seed growth and characterized by scanning electron  
22                    microscope (SEM), high-resolution transmission electron microscopy (HR-TEM), and  
23                    UV-vis spectra. Methamphetamine (METH) was used as an example to evaluate the  
24                    feasibility of the biosensor and to optimize the detection conditions. We demonstrated  
25                    that this sensing platform was able to detect as low as 0.1 nM (14.9 ng L<sup>-1</sup>) METH  
26                    with a negligible interference from other common illicit drugs. Various concentrations  
27                    of METH were spiked into urines, and the biosensor yielded recoveries more than  
28                    83.1%. In addition, the biosensor also showed a high sensitivity to detect cocaine.  
29                    These results demonstrated that the colorimetric sensor holds promise to be  
30                    implemented as a visual sensing platform to detect multiple illicit drugs in biological  
31                    samples and environmental matrices.

32                    **Keywords:** Au@Ag, Aptamer, Methamphetamine, Colorimetry, Illicit Drug

## 33 1. Introduction

34 Illicit drugs are widely abused and have become an increasing global concern [1-5].  
35 The United Nations Office of Drugs and Crimes has recently reported that illicit drugs  
36 had been used by a total of 246 million people, around 5 % of the global population  
37 aged between 15 and 64 [2]. Among these illicit drugs, cocaine (COC) is the primary  
38 drug of concern in Latin America/Caribbean and the second most used illegal  
39 substance in both Europe and United States[2, 3]. Methamphetamine (METH) is the  
40 second most widely abused drug in the world [6]. METH abuse has increased  
41 dramatically in the past years particularly in certain regions. For example, crystalline  
42 METH seizure has increased from around 7 tons in 2010 to 14 tons in 2013 in East  
43 and Southeast Asia [2]. The abuse of illicit drugs may cause severe societal  
44 consequences, such as loss of lives and health of abusers, increased treatment costs,  
45 and higher incidence of crimes [1-5].

46 The commercial analytical techniques include gas chromatography and high  
47 performance liquid chromatography-mass spectrometry [4, 5]. Although highly  
48 sensitive and selective, these techniques usually require expensive instruments and  
49 tedious sample pretreatment in laboratory such as solid phase extraction (SPE) or  
50 solid phase micro-extraction (SPME). Therefore, there is a great need to develop rapid,  
51 inexpensive, and sensitive tools to detect illicit drugs in order to monitor and control  
52 illicit drug abuse, preferably on the spot of sample collection.

53 Compared to conventional methods, biosensors hold promise to overcome the  
54 drawbacks of conventional analytical methods. A biosensor is a small device with a  
55 biological receptor that generates a signal (electrochemical, optical, nanomechanical,  
56 mass sensitive, etc.) in the presence of an analyte. Biosensors have the great potential  
57 for rapid and on-site detection of analytes in body fluids and environment samples,  
58 due to ease for miniaturization and capability of measuring complex matrices with  
59 minimal sample preparation[7-9]. In the past few decades, biosensors have been  
60 developed to measure numerous analytes in various matrices, such as heavy metals  
61 [10, 11], small molecule [12, 13], targeted DNA[14], peptides[15], enzyme[16],  
62 protein[15, 17], antigen [18], biomarkers[7, 8] and even bacteria[19, 20].

63 Aptamers have been attracted increasing attention as a biological receptor for  
64 biosensing, which is a sequence of oligonucleotides with high binding affinity and  
65 specificity to target utilizing the systematic evolution of ligands by exponential  
66 enrichment (SELEX) technology [21, 22]. Recently, efforts have been devoted toward  
67 the design of biosensors based on DNA aptamer for the detection of illicit drugs,  
68 especially for COC[23]. Most researchers use specific DNA aptamer to bind with  
69 COC, which generates a signal (electrochemical [24], colorimetry [25],  
70 fluorescence[26], SERS[27], *etc.*) in the presence of COC due to the conformation  
71 changes of DNA aptamers. Mokhtarzadeh *et al* [3] reviewed recent advances and  
72 applications of COC aptamer-based biosensors and nano-biosensors, which mainly  
73 focused on fluorescence, colorimetric and electrochemical techniques for the  
74 detection of COC. Besides COC, few other illicit drugs were reported using sensing  
75 technology. Mohsen *et al* [28, 29] firstly developed an electrochemical impedance

76 spectroscopic sensing for methamphetamine using a specific aptamer by SELEX. Shi  
77 *et.al* [30] developed a colorimetric and bare eye determination of urinary  
78 methylamphetamine based on aptamers and the salt-induced aggregation of  
79 unmodified gold nanoparticles. Yarbakht and co-workers [31] described the  
80 unmodified gold nanoparticles as a colorimetric probe for visual methamphetamine  
81 detection.

82 Nano notable metals, especially gold nanoparticles, have been used increasingly for  
83 biosensing application owing to their facile preparation and excellent optical  
84 properties [32-34]. These properties are utilized to develop many analytical methods  
85 including colorimetry[35, 36], light scattering[37, 38], scanometry [39, 40], surface  
86 enhanced Raman scattering [41] and chemiluminescence[42, 43]. In particular,  
87 colorimetry has particular advantages such as simplicity, low cost, and amenability[35,  
88 44]. The nano gold (AuNPs)-based colorimetric biosensor to detect oligonucleotides  
89 was first reported by Mirkin's group [32]. In their system,  
90 dispersed oligonucleotide-modified AuNPs were assembled into aggregated  
91 polymeric networks *via* hybridization with complementary target sequences. An  
92 obvious change in the surface plasmon resonance (SPR) absorption peak between  
93 dispersed and aggregated AuNPs was observed, leading to a significant red-to-blue  
94 color change which could be easily visualized by naked eyes[32, 44]. However, the  
95 efficiency of this method to detect lower concentration of targets was limited by the  
96 aggregation induced sedimentation [44]. To achieve highly sensitive assay, novel  
97 structures of AuNPs have been synthesized [45-47], for example, Au–Ag core–shell  
98 plasmonic nanoparticles (PNPs) as molecular probes for the detection of sulfide. This  
99 colorimetric assay allows for a linear logarithmic dependence on sulfide  
100 concentrations from 50 nM to 100  $\mu$ M [45]. Yan *et al* [46] designed a Au core-Ag  
101 shell nanostructures with embedding Cy5-labelled DNA aptamer to target  
102 chloramphenicol using surface-enhanced Raman scattering (SERS) for detection. This  
103 SERS-based sensor is able to detect as low as 0.19  $\text{pg mL}^{-1}$  chloramphenicol.  
104 However, to our knowledge, Au–Ag core–shell plasmonic nanoparticles (PNPs) have  
105 not yet been used for illicit drug detection.

106 In this paper, we developed a non-aggregated Au@Ag-based colorimetric strategy  
107 for illicit drugs detection using a reporter probe, capture probe and an aptamer.  
108 Au@Ag core-shell nanoparticles were synthesized by seeds growth to enhance SPR  
109 signal and detection sensitivity. The biosensor was optimized by varying the  
110 concentrations of magnetic beads and the aptamer, as well as the hybridization  
111 reaction time. Selectivity of the sensor was examined using 8 common illicit drugs  
112 other than METH. The optimized sensor was used to detect METH in urine specimens  
113 of drug addicts to evaluate recovery. This platform was also demonstrated to be  
114 capable of detection of other illicit drugs such as cocaine, indicating that it could be  
115 used as a generic approach for monitoring of illicit drugs.

## 116 **2. Materials and Methods**

### 117 **2.1. Materials**

118 HAuCl<sub>4</sub>·3H<sub>2</sub>O and AgNO<sub>3</sub> were purchased from Shanghai Chemical Reagent Co.,  
119 Ltd. (Shanghai, China). Carboxyl-coated magnetic beads (1.05 μm Dynabeads™  
120 MyOne™, 10 mg mL<sup>-1</sup>) were purchased from Invitrogen in Norway. Trisodium citrate  
121 was obtained from Sigma-Aldrich (USA). Oligonucleotide sequences showed in  
122 Table S1 were obtained from Sangon Biotech (Shanghai, China) Co. Ltd. and purified  
123 by HPLC. All illicit drugs and metabolites were purchased from Cerilliant (Round  
124 Rock, TX, USA). Urines of METH abusers were collected in Guangdong Province  
125 with the help of a local rehabilitation center. Urine sample collection and experiments  
126 were carried out in accordance with a protocol approved by the ethics committee of  
127 Peking University and with informed consent of the addicts. 0.22 μm membrane  
128 filters were purchased from ANPEL Laboratory Technologies (Shanghai, China) Inc.  
129 Ultra-pure water (18.2 MΩ) from a Millipore filtration system was used in all  
130 experiments. Following buffers were used: PB solution (10 mM phosphate sodium  
131 buffer solution, pH 7.4), PBS-T buffer (10 mM phosphate sodium buffer solution, pH  
132 7.4, 0.1 M NaCl, 0.05% tween-20), MES buffer (2-[N-morpholino]ethane sulfonic  
133 acid, 0.1 M, pH 4.8), and Tris buffer (2-amino-2-hydroxymethyl-1,3-propanediol, 50  
134 mM, pH 7.4).

## 135 **2.2. Synthesis of Au@Ag core-shell nanoparticles**

136 Gold nanoparticles were prepared by reduction of gold (III) chloride hydrate using  
137 trisodium citrate, following the procedure described in a previous publication[48] and  
138 with minor modifications. Briefly, 50 mL 0.01% (w/w) HAuCl<sub>4</sub> was reduced by 750  
139 μL 1% (w/w) trisodium citrate solution at 100 °C under vigorous magnetic stirring for  
140 15-20 min until the solution turned to be light red. The prepared red AuNPs particles  
141 were used as seed particles. Then 600 μL of AgNO<sub>3</sub> solution (0.5 %, w/w) was added  
142 to 100 mL boiling gold seed solution. Afterwards, 1 mL sodium citrate solution (1 %,  
143 w/w) was added dropwise as the reducing agent with stirring. The solution was boiled  
144 for 1 h and then cooled down to room temperature. The Au@Ag was characterized by  
145 Scanning Electron Microscope (SEM) (SIGMA, Germany), Transmissions Electron  
146 Microscope (TEM) (JEM-2100) and UV-vis spectrometer (Perk Elmer, USA), which  
147 confirms the successful synthesis of Au@Ag core-shell nanoparticles with a mean  
148 diameter of 40 nm.

## 149 **2.3. Preparation of reporter and capture probe**

150 The reporter probe was derived by modifying the synthesized Au@Ag core-shell  
151 nanoparticles with a RP DNA sequence that was partially complementary to the  
152 aptamer. The Au@Ag core-shell nanoparticles suspended in 5 ml PB buffer (pH 7.4,  
153 10 mM phosphate) were loaded with 15 nM thiol-functionalized reporter probes[49].  
154 After 24 h, 2 M NaCl was added to the solution to generate an overall NaCl  
155 concentration at 0.05 M, and then increased to 0.1 M after standing for 8 h. Upon  
156 aging in 0.1 M salt for additional 40 h, the nanoparticles were isolated by  
157 centrifugation at 6500 rpm for 15 min and washed three times with PBS-T (pH 7.4, 10  
158 mM phosphate, 0.05% Tween-20).

159 The capture reporter was super paramagnetic magnetic beads (MBs) with a  
160 carboxyl-modified coating, which were conjugated with the capture probe DNA using  
161 the protocol suggested by the manufacturer. Before immobilization, 2.5 mL of  
162 carboxylated magnetic beads were washed twice with 2.5 mL of MES buffer (100  
163 mM, pH 4.8) and then resuspended in 250  $\mu$ L MES buffer (100 mM, pH 4.8). Next, a  
164 mixture of 36.2 nmol  $\text{NH}_2$ -modified capture DNA and 36.2  $\mu$ mol EDC•HCl in 100  $\mu$ L  
165 MES buffer was added to the washed magnetic beads and incubated overnight with  
166 gently shaking at room temperature. Finally, the coated MBs were incubated with 50  
167 mM Tris buffer (pH 7.4) for 15 min at room temperature with gentle shaking to  
168 quench the remaining activated carboxylic acid groups. The coated magnetic beads  
169 were washed for three times with 2.5 mL Tris buffer and then re-suspended in  
170 hybridization buffer (PBS-T) and stored at 4°C for use.

#### 171 **2.4. Elaboration of biosensors**

172 In this study, we try to develop a strategy for illicit drugs detection based on the  
173 non-aggregated Au@Ag. To explore the effectiveness of the strategy, a  
174 non-aggregated Au@Ag nanoprobe-based on METH was employed as a case study.  
175 METH (1  $\mu$ M, 10  $\mu$ L) was mixed with 10  $\mu$ L METH aptamer (200 nM) solutions,  
176 followed by introducing 20  $\mu$ L PBS-T buffer. After incubation for half an hour, 5  $\mu$ L  
177 CP (PBS-T buffer) and 50  $\mu$ L RP (PBS-T buffer) were then added to the solution and  
178 allowed to hybridize under gently vortexing for 90 min. The total volume was  
179 increased to 100  $\mu$ L in PBS-T buffer. After hybridization, the MBs with target-linked  
180 Au@Ag core-shell nanoparticles together with unreacted MBs were easily attracted to  
181 the bottom of the tube by applying a round magnet (diameter: 3 cm, thickness: 3 mm).  
182 After the separation, the SPR of the supernatant was measured by a Shimadzu  
183 UV-2550 with 80  $\mu$ L quartz micro-cuvette.

184 Control experiments were performed with following combinations: MBs + Au@Ag;  
185 MBs + Au@Ag + METH; MBs + Au@Ag + aptamer. In these experiments, each  
186 component was added at the same volumes and concentrations as in the presence of  
187 METH. The missing components were replaced by the PBS-T buffer to maintain a  
188 constant total volume (100  $\mu$ L).

#### 189 **2.5 Optimization of Biosensors**

190 The concentration of magnetic beads causes the change of the ratio between the  
191 capture probes and reporter probe, which has significant impacts on the sensitivity of  
192 the assay. In order to get the optimal concentration of magnetic beads, a series of MBs  
193 concentrations were tested in this experiment. The experimental process was the same  
194 as the control experimental procedure (MBs + Au@Ag + aptamer) mentioned above.  
195 The volume of MBs (10 mg/mL) was 0, 0.1  $\mu$ L, 0.5  $\mu$ L, 1, and 5  $\mu$ L.

196 Hybridization reaction time is an important parameter for colorimetric biosensor.  
197 We examined the reaction time of the hybridization by recording the peak intensities  
198 of SPR signal. The experimental process was also the same as the control  
199 experimental procedure described above. SPR signals were recorded every 15 min  
200 from 0 to 105 min.

201 The optimal concentration of METH aptamer was determined by measuring  
202 absorbance intensities at 400 nm. The biosensor was optimized using different  
203 concentrations of aptamer (0, 10 nM, 20 nM, 30 nM, 40 nM, 50 nM, and 60 nM),  
204 following the procedure for control experiments mentioned above.

## 205 **2.6 Evaluation of the analytical performance**

206 Under the optimized conditions, the sensitivity and linearity of the biosensor to  
207 detect METH were determined at METH concentrations from 0.50 nM to 200 nM.

208 The selectivity of the biosensor was evaluated by other 8 common illicit drugs and  
209 metabolites, namely ketamine (KET), norketamine (NK), morphine (MOR), cocaine  
210 (COC), cathinone (CAT), methcathinone (MCAT), 3-trifluoromethylphenylpiperazine  
211 (BZP), and 4,4'- two amino two phenyl methane (MDA). The experiment procedure  
212 was same as above, except that METH was replaced by other illicit drugs or  
213 metabolites. A much higher concentration (1  $\mu$ M) was used for other drugs and  
214 metabolites, whereas a METH concentration of 50 nM was used as control.

## 215 **2.7 Analysis of urine samples with biosensors**

216 To test the feasibility of detecting METH in biological samples, METH  
217 concentrations in urines were determined using the biosensor. An aliquot of 20 $\mu$ L of  
218 each urine samples were measured using our sensors after filtered with 0.22  $\mu$ m  
219 membrane filters. The measured concentrations were compared with those determined  
220 from high performance liquid chromatography-tandem mass spectrometer  
221 (HPLC-MS/MS) used a UFLCXR-LC system (Shimadzu, Japan) with a Phenomenex  
222 Gemini C18 column (100 mm 2 mm, 3  $\mu$ m) and an ABI 4000 triple quadrupole mass  
223 spectrometer (AB SCIEX, USA). For HPLC-MS/MS analysis, the urine samples  
224 were first diluted by MeOH by a factor of 6, vortexed for 20s, and centrifuged for 1  
225 min at 13000 rpm. Aliquots of supernatants, added with deuterated internal standards  
226 analyzed following conditions described elsewhere[4, 5]. To examine the recovery of  
227 METH, one of the urine samples was spiked with three concentrations (10, 50, and  
228 100 nM). The METH concentrations in spiked samples were then determined using  
229 the biosensor.

## 230 **2.8 Cocaine detection with biosensors**

231 In order to explore the universal applicability of our proposed strategy, another  
232 widely-used illicit drug, cocaine, was detected with the same approach. The detection  
233 followed the conditions for METH except with minor changes as follows: 1) the  
234 concentration of cocaine (COC) in the initial detection experiment and control  
235 experiment was 150 nM; 2) COC aptamer concentrations of 0, 5, 10,15, 20, 30, 40,  
236 and 50 nM were tested to find the optimal concentration; 3) COC concentrations 0,  
237 0.5, 1.0, 5.0, 10.0, 20.0, 40.0, 60.0, 80.0, 100.0, and 150.0 nM were tested to examine  
238 the sensitivity and linearity of the biosensor.

## 239 **3. Results and discussion**

### 240 **3.1 Characteristics of Au@Ag**

241 According to experimental results, a significant red-to-yellow color change  
242 between AuNPs and Au@Ag can be easily visualized by the naked eye. Figure 1A

243 showed that the average diameter of Au@Ag core-shell nanoparticle was  
244 approximately 40 nm. However, the contrast of the shell-silver nano particles is  
245 different from that of the core-AuNP in HR-TEM image (Figure 1B). The analysis of  
246 the UV-vis spectra (Figure 1 C) from AuNPs and Au@Ag core-shell nanoparticles  
247 show that the absorption peak ( $\lambda_{\max}$ ) shifted from 520 nm to 400 nm, indicating a blue  
248 shift. This is because AuNPs and Au@Ag have different frequencies of surface  
249 plasmon resonance (SPR) in spite of the same particle size. The shift in the SPR  
250 absorption peak between AuNPs and Au@Ag led to the significant red-to-yellow  
251 color change. The intensity of SPR signal from Au@Ag was much stronger than that  
252 from AuNPs even though at the same concentrations. Thus, Au@Ag is a better signal  
253 transducer compared to AuNPs.

### 254 **3.2 Feasibility of biosensor**

255 The designed mechanism of the new colorimetric sensor is illustrated in Scheme 1.  
256 The biosensor consisted of a reporter probe (RP) (Scheme 1A), a capture probe (CP)  
257 (Scheme 1B) and an aptamer (Apt). The reporter probe was derived by modifying the  
258 synthesized Au@Ag core-shell nanoparticles with a RP DNA sequence that was  
259 partially complementary to the aptamer (Scheme 1A). The capture reporter was super  
260 paramagnetic magnetic beads (MBs) with a carboxyl-modified coating, which can be  
261 functionalized with amine-modified oligonucleotides with  
262 1-ethyl-3-(3-dimethylaminopropyl) carbodiimide hydrochloride (EDC•HCl) as the  
263 linker (Scheme 1B). The amine-modified oligonucleotides are able to fully match one  
264 portion of a target sequence but are different from the fragment complementary with  
265 RP DNA. And these MBs were attracted by an external magnetic field and facilitate  
266 the sample separation activated by an external magnetic field. As is shown in Scheme  
267 1C, the aptamer could bind to reporter probe and capture probe to form  
268 Au@Ag-DNA-MBs sandwich structure through hybridization. The double-stranded  
269 DNA (dsDNA) was composed of both RP DNA and CP DNA complementary to the  
270 different DNA aptamer fragment. When an external magnetic field is applied, the  
271 sandwich structure complex is removed from the suspension, which reduces the  
272 intensity of SPR signal from Au@Ag core-shell nanoparticles [50, 51]. In contrast, in  
273 the presence of the target drugs, aptamer binding to the two probes is prevented and  
274 Au@Ag-DNA-MBs complex cannot be formed the aptamer which binds preferably  
275 with the target drug molecules due to higher affinity [28, 29]. Thus, the concentration  
276 of Au@Ag remaining in the supernatant is proportional to the concentrations of target  
277 drugs. As the amount of the target drug increased, the color of the supernatant  
278 changed from light yellow to deep yellow, which could be measured with UV-vis  
279 spectrometer and even be visualized by naked eye.

280 To test the feasibility of this strategy, effects of this analytical method with or  
281 without illicit drugs (e.g. METH) on the SPR signal of Au@Ag core-shell  
282 nanoparticles were determined. In the control experiment, an absolute absorbance  
283 intensity of 0.46 was observed (Figure 1D, MBs+Au@Ag). When METH was added  
284 to the system, the absorbance intensity has no significant change (Figure 1D,  
285 MBs+Au@Ag+METH), indicating that METH alone had no interference to this  
286 analytical system. When METH aptamer was added to the system, the absorbance



287 intensity decreased dramatically (Figure 1D, MBs+Au@Ag+Apt), due to the  
288 formation of the Au@Ag-dsDNA-MBs complex following the base pair matching  
289 principle to form dsDNA. The Au@Ag-dsDNA-MBs sandwiches could be removed  
290 by external magnetic field. The removal of Au@Ag core-shell nanoparticles led to  
291 a decrease in absorbance signal at 400 nm. When both METH and METH aptamer  
292 existed in this system, the absorbance was basically recovered (Figure 1D,  
293 MBs+Au@Ag+Apt+METH). The signal was only slightly lower than the value of  
294 absolute absorbance intensity of Au@Ag core-shell nanoparticles. The increase in  
295 absorbance in the presence of both METH aptamer and METH was due to formation  
296 of METH-aptamer complex. The complex blocked formation of the  
297 Au@Ag-DNA-MBs complex, which prevented removal of the Au@Ag core-shell  
298 nanoparticles by the external magnetic field.

299 According to our experimental results, (1) The color of the solution is always  
300 yellow and can only be reduced in magnitude in the presence of different  
301 concentration of METH (Figure 3C); (2) There is no complex spectrum in the  
302 presence of different concentration of METH (Figure 3A); (3) The peak of SPR signal  
303 is always at 400 nm, thus, there is no red shift or blue shift (Figure 3A). Thus, on this  
304 sensing platform, Au@Ag core-shell nanoparticles would bind specifically with  
305 magnetic particles without the formation of the Au@Ag aggregates. This simple  
306 design avoids the complex spectrum of the classical colorimetric biosensor based on  
307 nanoparticles aggregation[6]. The color of the solution is always yellow and can only  
308 be reduced in magnitude. Due to the stability of dispersed Au@Ag core-shell  
309 nanoparticles, one only needs to examine the change in intensity of their specific  
310 absorption peak rather than the complex spectra of aggregates. These results indicate  
311 that designed mechanism is effective to detect METH.

### 312 **3.3 Optimization of sensing conditions**

313 The concentration of magnetic beads has a significant effect on experimental result.  
314 Excessive magnetic beads would cause waste, whereas insufficient magnetic beads  
315 would have a significant impact on the sensitivity of biosensors. In order to get the  
316 optimal concentration of magnetic beads, sensitivity of colorimetric approach in the  
317 presence of various MBs was also monitored, and the minimum SPR signal was  
318 optimized as the experimental condition. The optimized concentration of the MBs was  
319 determined with unchanged concentration of reporter probes and METH aptamer. As  
320 shown in Figure 2A, optimized MBs volume to achieve highest sensitivity was around  
321 1  $\mu$ L.

322 The hybridization time to form Au@Ag-dsDNA-MBs is an important parameter for  
323 the evaluation of colorimetric approach. Aptamers were added at the time point of 0 s,  
324 and spectra changes were observed. After addition of METH aptamer, the SPR peak  
325 signals of Au@Ag core-shell nanoparticles were recorded for 110 min. Figure 2B  
326 shows that the intensity of SPR signal at 400 nm gradually decreased, and reached the  
327 minimum value in about 60 minutes. So the optimal reaction time is 60 minutes.

328 SPR signal of Au@Ag nanoparticles decreased with increasing concentrations of  
329 METH aptamer (Figure 2C). Near complete quenching occurred at a concentration of  
330 60 nM. It should be noted that the excessive usage of METH aptamer could result in

331 non-specific (i.e., no SPR enhancement) binding to the METH. As shown in Figure  
332 2C, at an aptamer concentration of 40 nM, METH prevented the quenching of the  
333 Au@Ag and SPR intensity of Au@Ag was almost fully recovered (up to 89.1%) to its  
334 initial value. Thus, 40 nM METH aptamer was chosen in our biosensor.

### 335 3.4 Evaluation of sensing performance

336 To determine the limit of detection (LOD) of our biosensors, different  
337 concentrations of METH from 0 to 200 nM were measured. Figure 3A shows the dose  
338 response of METH concentration with the colorimetric signal. As the METH  
339 concentrations increasing, the color of the supernatant solution turned from light  
340 yellow and to deep yellow (Figure 3C). The peak intensity of SPR signal is  
341 proportional to METH concentration, and the increasing METH concentration  
342 therefore leads to the deformation of Au@Ag-DNA-MBs sandwich structure. As is  
343 shown in Figure 3 B, the intensity of SPR signal ( $\lambda_{\max}=400$  nm) increased with the  
344 increasing METH concentrations, and the linear range was determined from 0.5 nM to  
345 200 nM ( $R^2=0.994$ ). The LOD of the biosensor was determined to be 0.1 nM ( $3\sigma$ ),  
346 which is much lower than  $1000 \text{ ng mL}^{-1}$  ( $6.7 \mu\text{M}$ ), the threshold of positive METH  
347 detection in urine samples recommended by the National Institute on Drug Abuse of  
348 United States[52]. Shi *et al.* developed a aptamer biosensor for the detection of  
349 METH based on gold nanoparticles with a LOD at  $0.82 \mu\text{M}$  [6]. Oghli *et al.* is able to  
350 electrochemically detect METH as low as 50 nM [53]. Compared to those sensors,  
351 our sensitivity is much improved and hold a great potential for routine screening of  
352 METH in urine samples

353 To examine the selectivity of our biosensor, 8 non-target illicit drugs and/or  
354 metabolites (KET, NK, MOR, COC, CAT, MCAT, BZP and MDA) were tested.  
355 Figure 4A showed the responses of the colorimetric assay of METH (50 nM) and  
356 other drugs or metabolites ( $1 \mu\text{M}$ ) under the optimized condition. METH led to an  
357 evident increase in the 400 nm value of the assay. In contrast, the absorbance signals  
358 associated with others compounds stayed at the same level as the blank. These signals  
359 were much lower than that in the presence of METH, despite the fact that METH  
360 concentration (50 nM) was much lower than other illicit drugs and/or metabolites.  
361 Furthermore, the enhancement in absorbance signals (relative to the blank) was not  
362 statistically significant among other drugs, These results demonstrate that binding  
363 affinity of METH to METH-aptamer were much stronger than that to all other illicit  
364 drugs, rendering the biosensor with high specificity toward METH.

365 In order to further investigate the potential application of the proposed sensor, the  
366 assay was employed to detect METH in urine samples. The average recovery of  
367 METH in spiked urine sampled ranged from 83.1 and 90.5% (Table 1). The METH  
368 concentrations measured using HPLC-MS/MS (Figure 4B, black bar) ranged from  
369 19.2 to 131.8 nM. METH concentrations (Figure 4B, red bar) analyzed using our  
370 biosensor fell within the same range, but were slightly lower than the  
371 HPLC-MS/MS-derived concentrations, probably due to matrix effect [4, 54-56]. The  
372 variation of the measured valued from our sensors and HPLC-MS/MS are less than  
373 8.7%, indicating that our sensors have a clear potential for the detection of METH in  
374 real biological samples.

### 375 **3.5 Detection of cocaine with biosensors**

376 The sensing platform was also used to detect cocaine to explore the feasibility of  
377 this strategy as a generic platform. The probe sequences (Table. S1) are composed of  
378 an aptamer for COC and two probes that are complementary to the cocaine aptamer in  
379 different regions. As expected, in the absence of COC, the SPR signal of the  
380 supernatant was much lower than absolute SPR signal of Au@Ag; however, in the  
381 presence of COC, the strong SPR signal nearly equal to the absolute SPR signal of  
382 Au@Ag was observed (Figure S2). Optimal concentration of COC aptamer was found  
383 to be 30 nM, which is less than that of METH aptamer (Figure S3). Furthermore, a  
384 log-linear relationship ( $R^2= 0.987$ ) between COC concentration and absorbance signal  
385 intensity was also observed in a COC concentration range from 1.0 nM to 150 nM.  
386 The LOD was 0.5 nM (Figure S4) and comparable with previous report[23]. The  
387 promising results clearly demonstrates the versatility of the non-aggregation Au@Ag  
388 colorimetric strategy for illicit drug detection.

### 389 **4. Conclusion**

390 A novel, cost-effective and label-free biosensor based on the non-aggregation  
391 Au@Ag was developed for illicit drugs detection. The biosensor consisted of a  
392 reporter probe that is a specific single-stranded DNA sequences coated with Au@Ag,  
393 a capture probe conjugated with superparamagnetic magnetic beads, and an illicit  
394 drug-binding DNA aptamer. The DNA aptamer could hybridize with both RP and CP,  
395 generating Au@Ag-DNA magnetic beads (MBs) sandwich structure. When an  
396 external magnetic field is applied, Au@Ag-DNA-MB is removed from the solution,  
397 leading to decreased SPR intensity. In the presence of the illicit drugs,  
398 Au@Ag-DNA-MB sandwich structure cannot be formed due to higher affinity of the  
399 aptamer to illicit drug than that to complementary ssDNA. SPR intensity is correlated  
400 with the concentrations of target illicit drugs and this correlation can be used to  
401 quantify the target drugs. We demonstrated the novel sensing platform for the  
402 detection of illicit drugs such as METH and COC.

403 The optimized biosensor is able to detect as low as 0.1 nM METH with a linear  
404 range of from 0.5 nM to 200 nM, and other non-specific illicit drugs show a  
405 negligible interference. Recoveries of METH in the spiked urine samples were  
406 evaluated to be more than 83.1%. We also use HPLC-MS/MS to analyze urine  
407 samples for validation, and the results are in agreement. Furthermore, the developed  
408 sensing platform was used for the detection of cocaine with the cocaine-binding  
409 aptamer, which shows a promising result and the universality of our biosensors. In  
410 summary, we have demonstrated a generic biosensor based on non-aggregation  
411 Au@Ag core-shell structure for the sensitive detection of METH and COC, and it  
412 also has a potential for monitoring a wide spectrum of targets including illicit drugs  
413 by replacing respective DNA aptamer.

### 414 **Acknowledgments**

415 We gratefully acknowledge the support from the National Natural Science  
416 Foundation of China (NSFC) (No. 41371442 and 41401566).

417

### 418 **References**

- 420 [1] S. Galanie, K. Thodey, I.J. Trenchard, I.M. Filsinger, C.D. Smolke, Complete biosynthesis of opioids in  
421 yeast, *Science* 349(6252) (2015) 1095-100.
- 422 [2] U.N.O.D.a. Crime, *World Drug Report 2015* (2015).
- 423 [3] A. Mokhtarzadeh, J.E.N. Dolatabadi, K. Abnous, M.D.L. Guardia, M. Ramezani, Nanomaterial-based  
424 cocaine aptasensors, *Biosensors & Bioelectronics* 68(68) (2015) 95-106.
- 425 [4] P. Du, K. Li, J. Li, Z. Xu, X. Fu, J. Yang, H. Zhang, X. Li, Methamphetamine and ketamine use in major  
426 Chinese cities, a nationwide reconnaissance through sewage-based epidemiology, *Water Research* 84  
427 (2015) 76-84.
- 428 [5] B. Subedi, K. Kannan, Mass loading and removal of select illicit drugs in two wastewater treatment  
429 plants in New York State and estimation of illicit drug usage in communities through wastewater  
430 analysis, *Environmental Science & Technology* 48(12) (2014) 6661-6670.
- 431 [6] Q. Shi, Y. Shi, Y. Pan, Z. Yue, H. Zhang, C. Yi, Colorimetric and bare eye determination of urinary  
432 methylamphetamine based on the use of aptamers and the salt-induced aggregation of unmodified  
433 gold nanoparticles, *Microchimica Acta* 182(3-4) (2015) 505-511.
- 434 [7] Z. Yang, M.A. D'Auriac, S. Goggins, B. Kasprzyk-Hordern, K.V. Thomas, C.G. Frost, P. Estrela, A Novel  
435 DNA Biosensor Using a Ferrocenyl Intercalator Applied to the Potential Detection of Human  
436 Population Biomarkers in Wastewater, *Environmental Science & Technology* 49(9) (2015).
- 437 [8] R.D.L. Rica, M.M. Stevens, Plasmonic ELISA for the ultrasensitive detection of disease biomarkers  
438 with the naked eye, *Nature Nanotechnology* 7(12) (2012) 821-824.
- 439 [9] Z. Yang, B. Kasprzyk-Hordern, C.G. Frost, P. Estrela, K.V. Thomas, Community Sewage Sensors for  
440 Monitoring Public Health, *Environmental Science & Technology* 49(10) (2015) 5845-5846.
- 441 [10] K. Mao, Z. Wu, Y. Chen, X. Zhou, A. Shen, J. Hu, A novel biosensor based on single-layer MoS<sub>2</sub>  
442 nanosheets for detection of Ag<sup>+</sup>, *Talanta* 132 (2015) 658-663.
- 443 [11] F.W. †, R.O. †, I. Willner, Detection of Metal Ions (Cu<sup>2+</sup>, Hg<sup>2+</sup>) and Cocaine by Using Ligation  
444 DNAzyme Machinery, *Chemistry - A European Journal* 18(50) (2012) 16030-6.
- 445 [12] Q. Li, Y.D. Wang, G.L. Shen, H. Tang, R.Q. Yu, J.H. Jiang, Split aptamer mediated endonuclease  
446 amplification for small-molecule detection, *Chemical Communications* 51(20) (2015) 4196-9.
- 447 [13] M.A.D. Neves, C. Blaszykowski, S. Bokhari, M. Thompson, Ultra-high frequency piezoelectric  
448 aptasensor for the label-free detection of cocaine, *Biosensors & Bioelectronics* 72 (2015) 383-392.
- 449 [14] Z. Yang, d.A.M. Anglès, S. Goggins, B. Kasprzykhordern, K.V. Thomas, C.G. Frost, P. Estrela, A novel  
450 DNA biosensor using a ferrocenyl intercalator applied to the potential detection of human population  
451 biomarkers in wastewater, *Environmental Science & Technology* 49(9) (2015) 5609-17.
- 452 [15] A.B. Iliuk, L. Hu, W.A. Tao, A. Chem., Aptamer in bioanalytical applications, *Analytical Chemistry*  
453 83(12) (2011) 4440-52.
- 454 [16] Z. Wu, Y. Liu, X. Zhou, A. Shen, J. Hu, A "turn-off" SERS-based detection platform for ultrasensitive  
455 detection of thrombin based on enzymatic assays, *Biosensors and Bioelectronics* 44 (2013) 10-15.
- 456 [17] J. Das, K.B. Cederquist, A.A. Zaragoza, P.E. Lee, E.H. Sargent, S.O. Kelley, An ultrasensitive universal  
457 detector based on neutralizer displacement, *Nature Chemistry* 4(8) (2012) 642-648.
- 458 [18] M.A. Najeeb, Z. Ahmad, R.A. Shakoor, A.M.A. Mohamed, R. Kahraman, A novel classification of  
459 prostate specific antigen (PSA) biosensors based on transducing elements, *Talanta* 168 (2017) 52-61.
- 460 [19] K. Saha, S.S. Agasti, C. Kim, X. Li, V.M. Rotello, Gold nanoparticles in chemical and biological  
461 sensing, *Chemical Reviews* 112(5) (2012) 2739-2779.
- 462 [20] P.D. Howes, R. Chandrawati, M.M. Stevens, Colloidal nanoparticles as advanced biological sensors,

463 Science 346(6205) (2014).  
464 [21] S.M. Shamah, J.M. Healy, S.T. Cload, Complex Target SELEX, *Accounts of Chemical Research* 41(1)  
465 (2008) 130-138.  
466 [22] N. Duan, W. Gong, S. Wu, Z. Wang, Selection and Application of ssDNA Aptamers against  
467 Clenbuterol Hydrochloride Based on ssDNA Library Immobilized SELEX, *Journal of Agricultural and*  
468 *Food Chemistry* 65(8) (2017) 1771-1777.  
469 [23] Z. Yang, E. Castrignanò, P. Estrela, C.G. Frost, B. Kasprzykhordern, *Community Sewage Sensors*  
470 *towards Evaluation of Drug Use Trends: Detection of Cocaine in Wastewater with DNA-Directed*  
471 *Immobilization Aptamer Sensors, Scientific Reports* 6 (2016).  
472 [24] Z. Yang, E. Castrignanò, P. Estrela, C.G. Frost, B. Kasprzyk-Hordern, *Community Sewage Sensors*  
473 *towards Evaluation of Drug Use Trends: Detection of Cocaine in Wastewater with DNA-Directed*  
474 *Immobilization Aptamer Sensors, Scientific Reports* 6 (2016).  
475 [25] M.N.S. And, D.W. Landry, Aptamer-Based Colorimetric Probe for Cocaine, *Journal of the American*  
476 *Chemical Society* 124(33) (2002) 9678-9.  
477 [26] M.N. Stojanovic, P.D.P. And, D.W. Landry, Aptamer-Based Folding Fluorescent Sensor for Cocaine,  
478 *Journal of the American Chemical Society* 123(21) (2001) 4928-31.  
479 [27] M. Oroval, M. Coronado-Puchau, J. Langer, M.N. Sanz-Ortiz, Á. Ribes, E. Aznar, C. Coll, M.D.  
480 Marcos, F. Sancenón, L.M. Liz-Marzán, Surface Enhanced Raman Scattering and Gated Materials for  
481 Sensing Applications: The Ultrasensitive Detection of Mycoplasma and Cocaine, *Chemistry* (2016).  
482 [28] M. Ebrahimi, M. Johariahar, H. Hamzeiy, J. Barar, O. Mashinchian, Y. Omid, Electrochemical  
483 impedance spectroscopic sensing of methamphetamine by a specific aptamer, *Bioimpacts Bi* 2(2)  
484 (2012) 91-5.  
485 [29] M. Ebrahimi, H. Hamzeiy, J. Barar, A. Barzegari, Y. Omid, Systematic Evolution of Ligands by  
486 Exponential Enrichment Selection of Specific Aptamer for Sensing of Methamphetamine, *Sensor*  
487 *Letters* volume 11(3) (2013) 566-570(5).  
488 [30] Q. Shi, Y. Shi, Y. Pan, Z. Yue, H. Zhang, C. Yi, Colorimetric and bare eye determination of urinary  
489 methylamphetamine based on the use of aptamers and the salt-induced aggregation of unmodified  
490 gold nanoparticles, *Microchimica Acta* 182(3) (2015) 505-511.  
491 [31] M. Yarbakht, M. Nikkhah, Unmodified gold nanoparticles as a colorimetric probe for visual  
492 methamphetamine detection, *Journal of Experimental Nanoscience* 11 (2015) 1-9.  
493 [32] R. Elghanian, J.J. Storhoff, R.C. Mucic, R.L. Letsinger, C.A. Mirkin, Selective colorimetric detection  
494 of polynucleotides based on the distance-dependent optical properties of gold nanoparticles, *Science*  
495 277(5329) (1997) 1078-1081.  
496 [33] K. Mao, Y. Chen, Z. Wu, X. Zhou, A. Shen, J. Hu, Catalytic Strategy for Efficient Degradation of  
497 Nitroaromatic Pesticides by Using Gold Nanoflower, *Journal of Agricultural and Food Chemistry* 62(44)  
498 (2014) 10638-10645.  
499 [34] D. Liu, Z. Wang, X. Jiang, Gold nanoparticles for the colorimetric and fluorescent detection of ions  
500 and small organic molecules, *Nanoscale* 3(4) (2011) 1421-33.  
501 [35] I.R.R. De, M.M. Stevens, Plasmonic ELISA for the ultrasensitive detection of disease biomarkers  
502 with the naked eye, *Nature Nanotechnology* 7(12) (2012) 821-4.  
503 [36] Y. Mao, T. Fan, R. Gysbers, Y. Tan, F. Liu, S. Lin, Y. Jiang, A simple and sensitive aptasensor for  
504 colorimetric detection of adenosine triphosphate based on unmodified gold nanoparticles, *Talanta*  
505 168 (2017) 279-285.  
506 [37] J. Li, S. Song, D. Li, Y. Su, Q. Huang, Y. Zhao, C. Fan, Multi-functional crosslinked Au nanoaggregates

507 for the amplified optical DNA detection, *Biosensors and Bioelectronics* 24(11) (2009) 3311-3315.

508 [38] X. Xu, D.G. Georganopoulou, H.D. Hill, C.A. Mirkin, Homogeneous Detection of Nucleic Acids  
509 Based upon the Light Scattering Properties of Silver-Coated Nanoparticle Probes, *Analytical Chemistry*  
510 79(17) (2007) 6650-6654.

511 [39] T.A. Taton, C.A. Mirkin, R.L. Letsinger, Scanometric DNA Array Detection with Nanoparticle Probes,  
512 *Science* 289(5485) (2000) 1757-1760.

513 [40] D. Kim, W.L. Daniel, C.A. Mirkin, Microarray-Based Multiplexed Scanometric Immunoassay for  
514 Protein Cancer Markers Using Gold Nanoparticle Probes, *Analytical Chemistry* 81(21) (2009)  
515 9183-9187.

516 [41] Y.C. Cao, R. Jin, C.A. Mirkin, Nanoparticles with Raman spectroscopic fingerprints for DNA and  
517 RNA detection, *Science* 297(5586) (2002) 1536-40.

518 [42] J. Wang, Y. Cao, Y. Xu, G. Li, Colorimetric multiplexed immunoassay for sequential detection of  
519 tumor markers, *Biosensors and Bioelectronics* 25(2) (2009) 532-536.

520 [43] L. Song, K. Mao, X. Zhou, J. Hu, A novel biosensor based on Au@Ag core-shell nanoparticles for  
521 SERS detection of arsenic (III), *Talanta* 146 (2016) 285-290.

522 [44] R.A. Reynolds, C.A. Mirkin, R.L. Letsinger, Homogeneous, Nanoparticle-Based Quantitative  
523 Colorimetric Detection of Oligonucleotides, *Journal of the American Chemical Society* 122(15) (2000)  
524 3795-3796.

525 [45] W. Yan, L. Yang, H. Zhuang, H. Wu, J. Zhang, Engineered "hot" core-shell nanostructures for  
526 patterned detection of chloramphenicol, *Biosensors and Bioelectronics* 78 (2016) 67-72.

527 [46] J. Hao, B. Xiong, X.D. Cheng, Y. He, E.S. Yeung, A. Chem, High-throughput sulfide sensing with  
528 colorimetric analysis of single Au-Ag core-shell nanoparticles, *Analytical Chemistry* 86(10) (2014)  
529 4663-7.

530 [47] T. Li, Y. Li, Y. Zhang, C. Dong, Z. Shen, A. Wu, A colorimetric nitrite detection system with excellent  
531 selectivity and high sensitivity based on Ag@Au nanoparticles, *Analyst* 140(4) (2015) 1076-81.

532 [48] A. Shen, L. Chen, W. Xie, J. Hu, A. Zeng, R. Richards, J. Hu, Triplex Au-Ag-C Core-Shell  
533 Nanoparticles as a Novel Raman Label, *Advanced Functional Materials* 20(6) (2010) 969-975.

534 [49] S.J. Hurst, A.K.R. Lyttonjean, C.A. Mirkin, Maximizing DNA Loading on a Range of Gold  
535 Nanoparticle Sizes, *Analytical Chemistry* 78(24) (2006) 8313-8.

536 [50] J.-J. Wang, Y.-Z. Jiang, Y. Lin, L. Wen, C. Lv, Z.-L. Zhang, G. Chen, D.-W. Pang, Simultaneous  
537 Point-of-Care Detection of Enterovirus 71 and Coxsackievirus B3, *Analytical Chemistry* 87(21) (2015)  
538 11105-11112.

539 [51] Y. Liu, Z. Wu, G. Zhou, Z. He, X. Zhou, A. Shen, J. Hu, Simple, rapid, homogeneous oligonucleotides  
540 colorimetric detection based on non-aggregated gold nanoparticles, *Chemical Communications* 48(26)  
541 (2012) 3164-6.

542 [52] R.L. Hawks, C.N. Chiang, Urine testing for drugs of abuse, *Nida Research Monograph* 73(2) (1986)  
543 1.

544 [53] A.H. Oghli, E. Alipour, M. Asadzadeh, Development of a novel voltammetric sensor for the  
545 determination of methamphetamine in biological samples on the pretreated pencil graphite electrode,  
546 *Rsc Advances* 5 (2015) 9674-9682.

547 [54] Y. Aminot, X. Litrico, M. Chambolle, C. Arnaud, P. Pardon, H. Budzinski, Development and  
548 application of a multi-residue method for the determination of 53 pharmaceuticals in water, sediment,  
549 and suspended solids using liquid chromatography-tandem mass spectrometry, *Analytical and*  
550 *Bioanalytical Chemistry* 407(28) (2015) 8585-8604.

551 [55] C. Boix, M. Ibáñez, J.V. Sancho, J. Rambla, J.L. Aranda, S. Ballester, F. Hernández, Fast  
552 determination of 40 drugs in water using large volume direct injection liquid chromatography–tandem  
553 mass spectrometry, *Talanta* 131 (2015) 719-727.

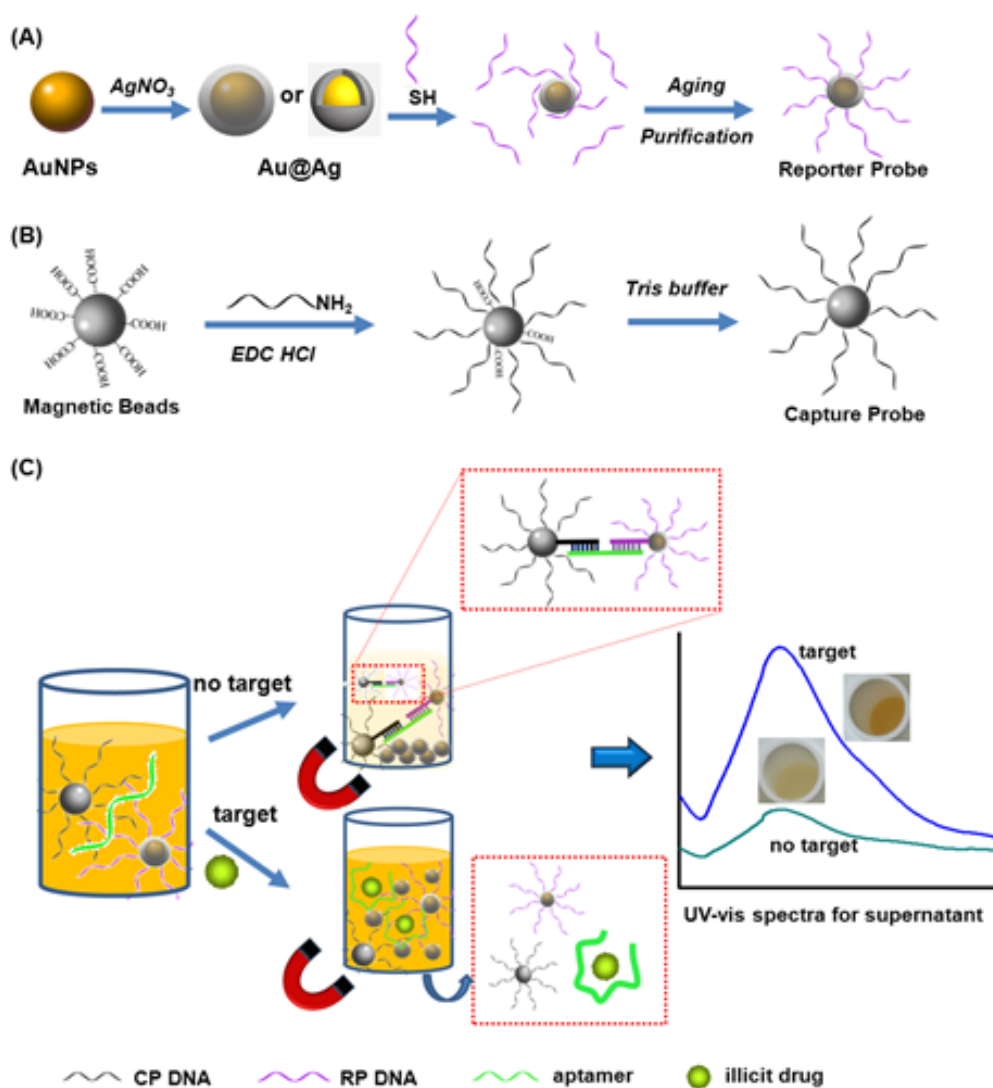
554 [56] P. Gago-Ferrero, V. Borova, M.E. Dasenaki, N.S. Thomaidis, Simultaneous determination of 148  
555 pharmaceuticals and illicit drugs in sewage sludge based on ultrasound-assisted extraction and liquid  
556 chromatography–tandem mass spectrometry, *Analytical and Bioanalytical Chemistry* 407(15) (2015)  
557 4287-4297.

558

559

560

561 **Figure:**



562

563

564

565 Scheme 1. The schematic representations of preparation of reporter probe (A) and  
566 capture probe (B) and colorimetric detection of illicit drug based on non-aggravation  
567 Au@Ag core-shell nanoparticles (C).

568

569

570

571

572

573

574

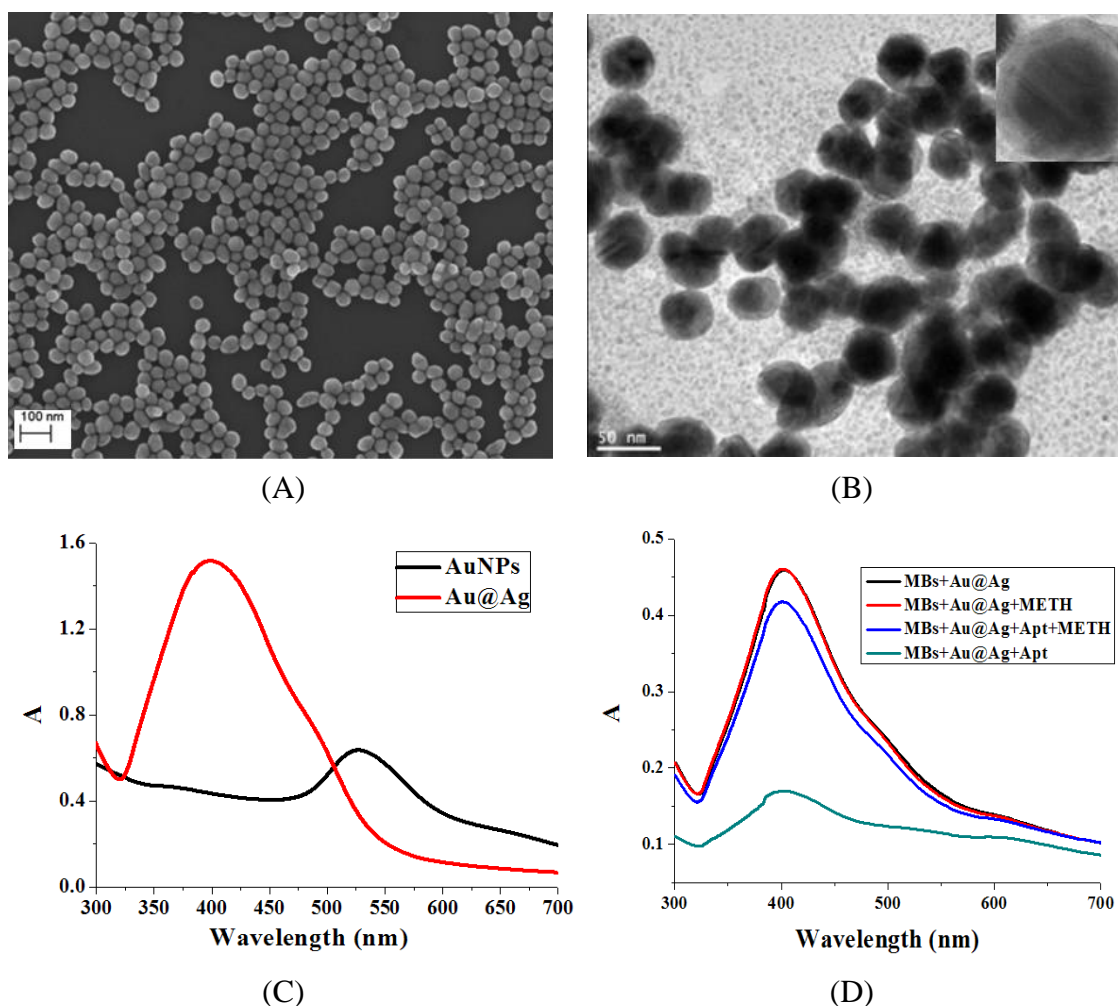
575

576



577

578

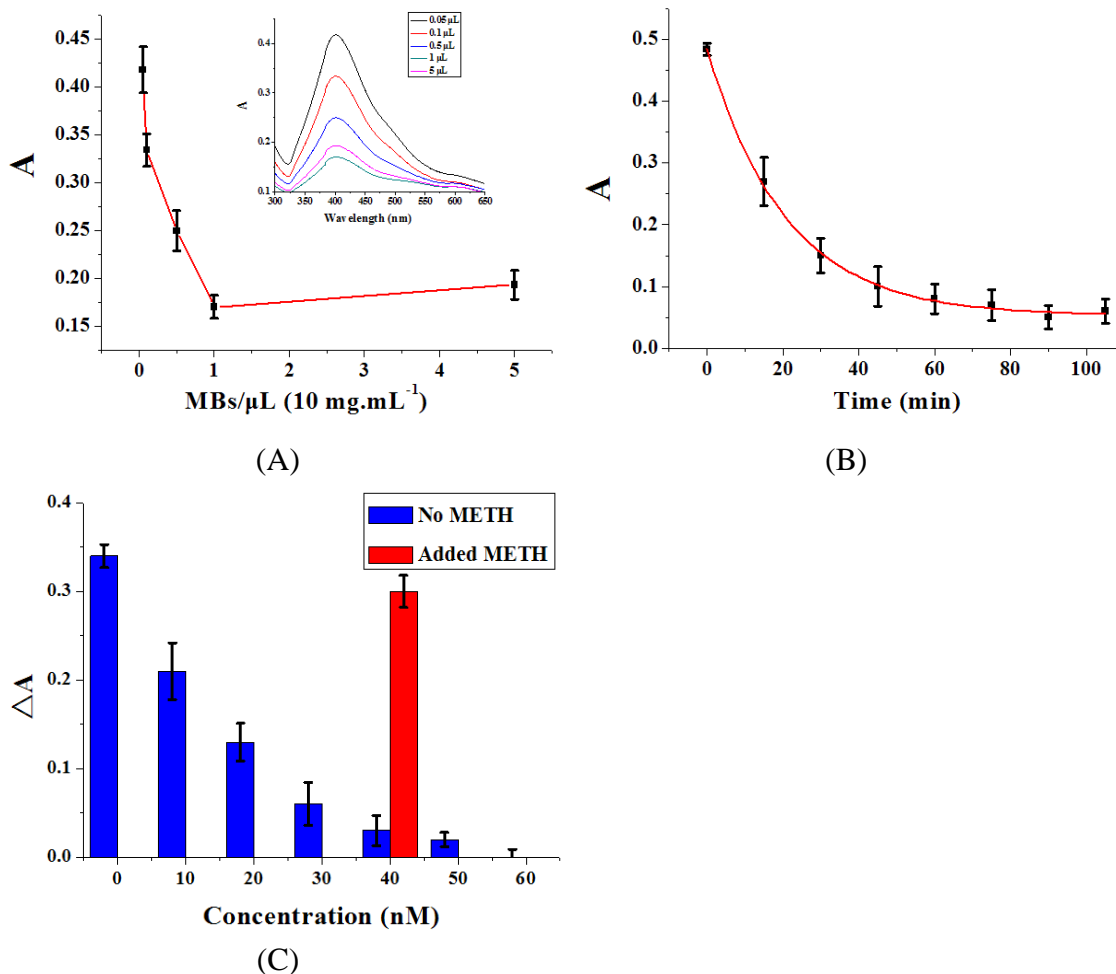


579 Figure 1. (A) Scanning electron microscope (SEM) image and (B) high resolution  
580 transmission emission microscope (HR-TEM) image of prepared Au@Ag core-shell  
581 nanoparticles. (C) SPR signal of Au@Ag and AuNPs. (D) UV-vis spectra of Au@Ag  
582 in the presence or absence of METH. The signal (A) is the absorbance of Au@Ag  
583 core-shell nanoparticles and error bars represent triplicate measurements (same for  
584 below).

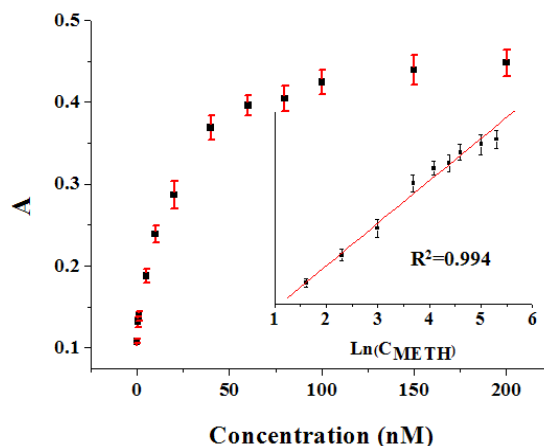
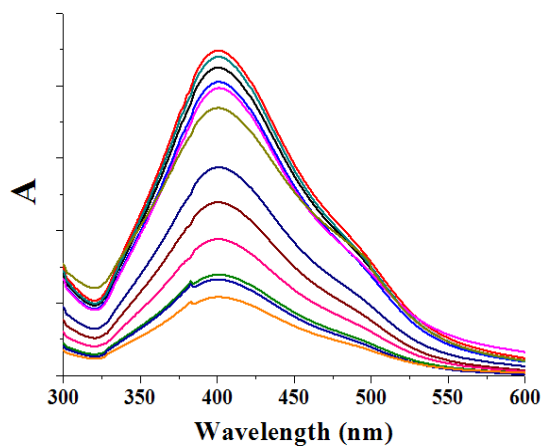
585

586

587



588 Figure 2. (A) SPR signal intensities at different MBs concentrations. The curve and  
589 UV-vis spectra (insert) of the supernatant at different concentrations of MBs. Under  
590 the same concentration of METH aptamer (40 nM), the sensitivity of assay positively  
591 correlated with variation of SPR peak intensity. (B) Hybridization reaction time of  
592 SPR signal intensity change at 400 nm with METH aptamer concentration of 40 nM.  
593 (C) SPR signal intensities of the Au@Ag ( $\lambda_{\text{max}}=400 \text{ nm}$ ) in the presence of different  
594 concentrations of METH aptamer (Blue). Red bar is SPR signal intensity of the  
595 Au@Ag in the presence of METH (100 nM). The signal ( $\Delta A$ ) is expressed as the  
596 relative absorbance with respect to the blank and error bars represent three replicate  
597 measurements (same for below).  
598



599  
600

(A)

(B)

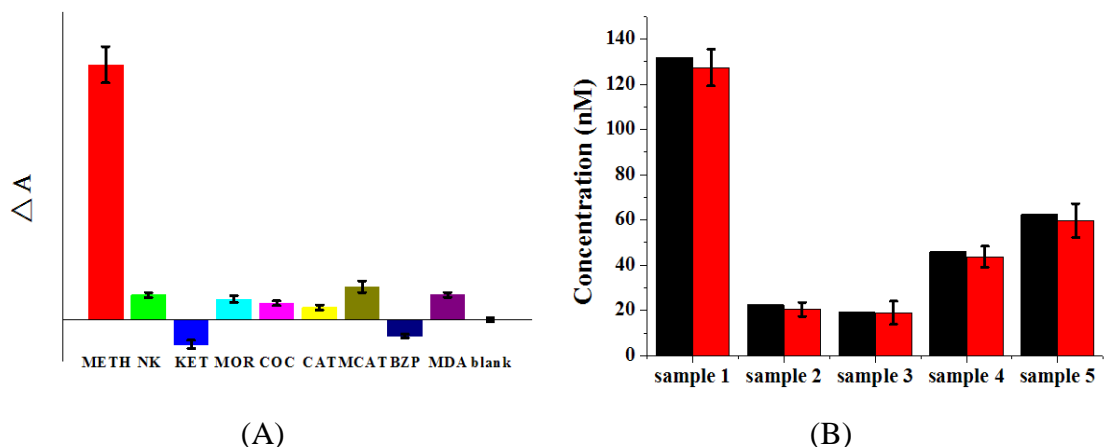


601

(C)

602

603 Figure 3. (A) UV-vis spectra of Au@Ag in the presence of different concentrations  
 604 of METH (from bottom to up: 0, 0.5, 1, 5, 10, 20, 40, 60, 80, 100, 150, 200 nM). (B)  
 605 SPR signal intensity ( $\lambda_{\max}=400$  nm) at various METH concentrations (The inset shows  
 606 the logarithm linear range concentration (0.5-200.0 nM)). (C) Color change of the  
 607 non-aggravation Au@Ag in the presence of METH. The METH concentrations in  
 608 tubes from left to right were: 0, 5, 10, 50, and 100 nM.



(A)

(B)

609 Figure 4. (A) Selectivity of the non-aggravation Au@Ag core-shell nanoparticles for  
 610 METH detection. The METH concentration was 50 nM, while the concentration of  
 611 other illicit drugs was 1  $\mu$ M. From left to right: METH, KET, NK, MOR, COC, CAT,  
 612 MCAT, BZP, MDA, and blank; (B) METH concentrations in human urine samples  
 613 measured by the biosensor and (red) and by HPLC-MS/MS (black).

614

615

616 Table 1. Recovery of METH in urines at three spiked METH concentration (10.0,  
 617 50.0 and 100.0 nM), respectively.

Spiked concentration (nM)	The measured concentration of METH (nM)				Rate of standard recovery (%)			
	1	2	3	Average	1	2	3	Average
0	19.23	18.74	18.85	18.94	-	-	-	-
10	27.35	27.75	26.64	27.25	81.2	90.1	77.9	83.1
50	64.30	59.30	65.80	63.13	90.1	81.1	93.9	88.4
100	113.40	109.50	105.30	109.40	94.2	90.8	86.5	90.5

618

## **Supporting information**

# **A Novel Colorimetric Biosensor Based on non-Aggregated Au@Ag Core–Shell Nanoparticles for Methamphetamine and Cocaine Detection**

***Kang Mao<sup>a</sup>, Zhugen Yang<sup>b</sup>, Junrong Li<sup>c</sup>, Xiaodong Zhou<sup>c</sup>, Xiqing Li<sup>a,\*</sup> and Jiming Hu<sup>c</sup>***

*<sup>a</sup> Laboratory for Earth Surface Processes, College of Urban and Environmental Sciences, Peking University, Beijing 100871, China*

*<sup>b</sup> Division of Biomedical Engineering, School of Engineering, University of Glasgow, Oakfield Road, Glasgow G12 8LT, United Kingdom*

*<sup>c</sup> Key Laboratory of Analytical Chemistry for Biology and Medicine (Ministry of Education), College of Chemistry and Molecular Sciences, Wuhan University, Wuhan 430072, China*

## Supplementary Materials

Table S1. Oligonucleotide sequences used in the experiment <sup>1</sup>.

METH RP DNA	5'-GAGTCCCACCTTGCAACCGT-SH-3'
COC RP DNA	5'-GGATTTATCCTTGTCTCCC-SH-3'
METH CP DNA	5'-NH <sub>2</sub> -CCAAATTACCCAGCCTACC-3'
COC CP DNA	5'-NH <sub>2</sub> -TATCGACCCACTTCATTCG-3'
METH aptamer	5'-ACGGTTGCAAGTGGGACTCTGGTAGGCTGGGTAATTTGG-3'
COC aptamer	5'-GGGAGACAAGGATAAATCCTTCAATGAAGTGGGTCGATA-3'

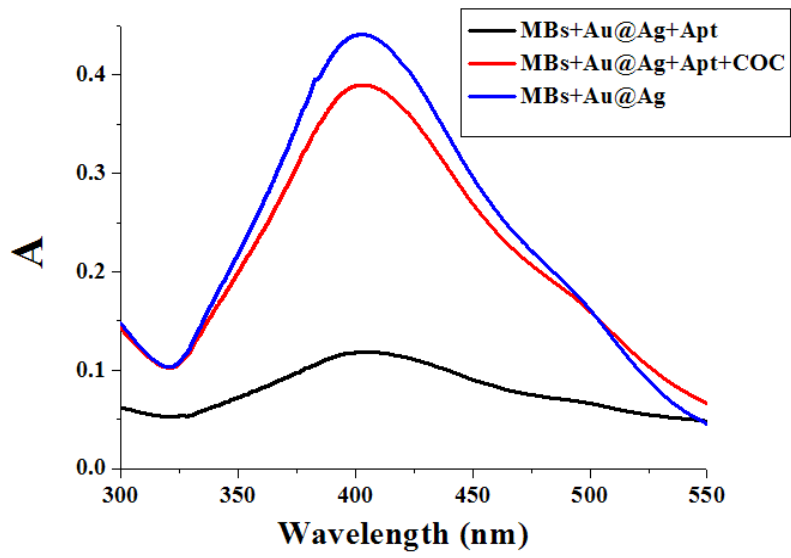


Figure S1. UV-vis spectra of Au@Ag in the presence or absence of COC.



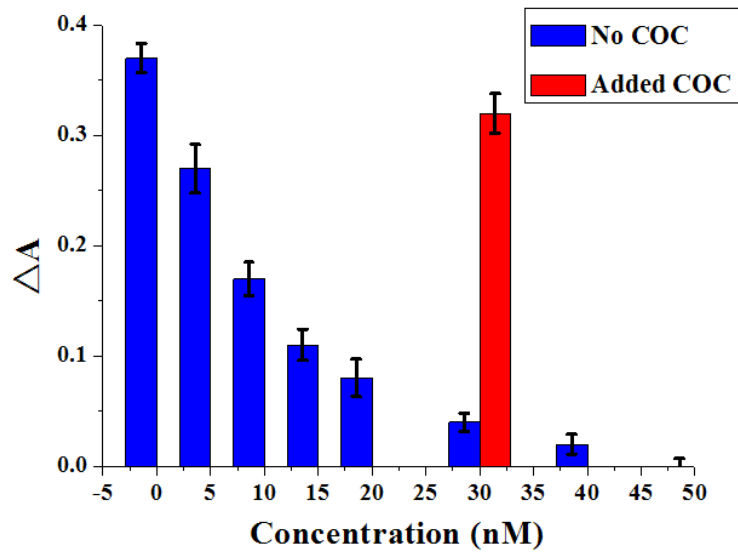


Figure S2. SPR signal intensities of the Au@Ag ( $\lambda_{\max}=400$  nm) in the presence of different concentrations of COC aptamer (Blue). Red bar is SPR signal intensity of the Au@Ag in the presence of COC (150 nM). The signal ( $\Delta A$ ) is expressed as the relative absorbance with respect to the blank and error bars represent three replicate measurements (same for below).

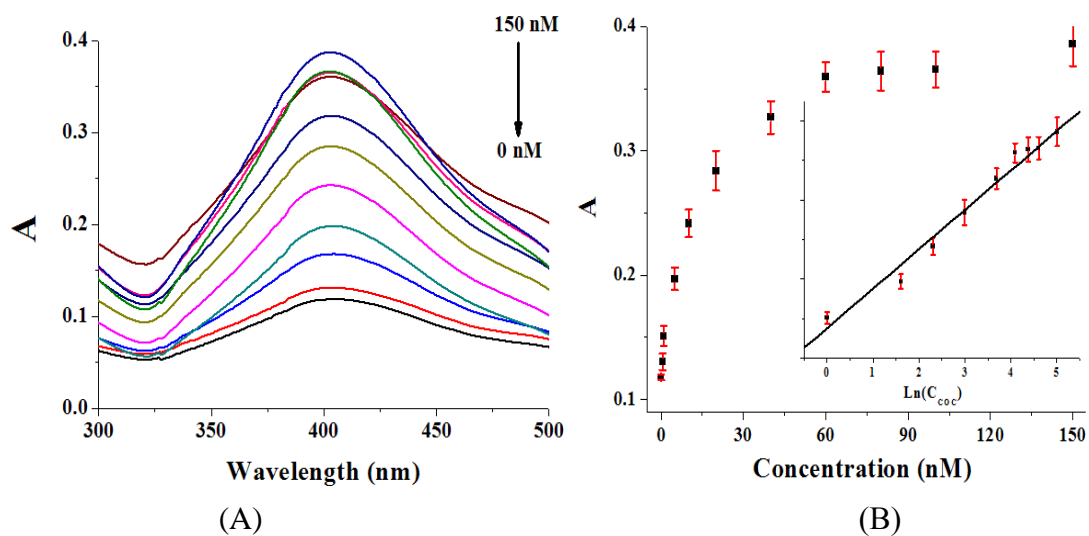


Figure S3. (A) UV-vis spectra of Au@Ag at different concentrations of COC (0, 0.5, 1, 5, 10, 20, 40, 60, 80, 100, and 150 nM). (B) SPR signal intensity ( $\lambda_{\max}=400$  nm) at various METH concentrations (The inset shows the logarithm linear range concentration (1.0-150.0 nM)).

## References

1. (a) Mao, K.; Yang, Z.; Du, P.; Xu, Z.; Wang, Z.; Li, X., G-quadruplex-hemin DNAzyme molecular beacon probe for the detection of methamphetamine. *Rsc Advances* **2016**, *6* (67); (b) Yang, Z.; Castrignanò, E.; Estrela, P.; Frost, C. G.; Kasprzyk-Hordern, B., Community Sewage Sensors towards Evaluation of Drug Use Trends: Detection of Cocaine in Wastewater with DNA-Directed Immobilization Aptamer Sensors. *Scientific Reports* **2016**, *6*, 21024.